

Summer 2021

An Investigation of Strong Electrostatic Adsorption Using Formed Commercial Supports

Connor Brendan McDonough

Follow this and additional works at: <https://scholarcommons.sc.edu/etd>



Part of the [Chemical Engineering Commons](#)

Recommended Citation

McDonough, C. B.(2021). *An Investigation of Strong Electrostatic Adsorption Using Formed Commercial Supports*. (Master's thesis). Retrieved from <https://scholarcommons.sc.edu/etd/6460>

This Open Access Thesis is brought to you by Scholar Commons. It has been accepted for inclusion in Theses and Dissertations by an authorized administrator of Scholar Commons. For more information, please contact digres@mailbox.sc.edu.

AN INVESTIGATION OF STRONG ELECTROSTATIC ADSORPTION USING
FORMED COMMERCIAL SUPPORTS

by

Connor Brendan McDonough

Bachelor of Science in Engineering
University of South Carolina, 2020

Submitted in Partial Fulfillment of the Requirements

For the Degree of Master of Science in

Chemical Engineering

College of Engineering and Computing

University of South Carolina

2021

Accepted by:

John R. Monnier, Director of Thesis

John R. Regalbuto, Reader

Christopher T. Williams, Reader

Melissa A. Moss, Reader

Tracey L. Weldon, Interim Vice Provost and Dean of the Graduate School

Abstract

Strong electrostatic adsorption (SEA) is a well-tested procedure for the synthesis of supported monometallic and bimetallic nanoparticles with ultrasmall size (< 2 nm). Where, previous studies have laid the foundation for SEA using a variety of powdered supports, catalysts in this form are not suited for large volume chemical applications where pressure drop is critical to the process economics. Although there is no fundamental difference between the surface functional groups on powdered and extruded supports, the present study examined electrostatic adsorption as it relates to proton diffusion, precursor diffusion, and capillary imbibition.

Three formed alumina spheres and one carbon extrudate were selected for study. The alumina spheres, provided by BASF, were developmental materials with varying pore size distributions between 12 and 24800 angstroms. The carbon, provided by ADM and manufactured by CABOT, was strictly microporous in structure and was included to investigate the differences in mass transport as a function of support material.

Results indicated, a significant limitation in the approach to pH equilibrium comparing formed alumina spheres with the same material crushed and sieved to a <44 μm powder. Experimental rate constants showed that the rate of surface protonation trends with larger pore diameters suggesting mass transport effects. Based on these findings, the analysis was expanded to include metal adsorption using chloroplatinic acid (CPA) as a Pt source. Where prior work using alumina samples with differing phase and surface areas

showed a common max Pt uptake of $1.7 \mu\text{mol}/\text{m}^2\text{-sup}$, the crushed alumina spheres in this study had a maximum loading of $0.8 \mu\text{mol}/\text{m}^2\text{-sup}$. A similar result was observed for carbon where prior work showed a maximum uptake of $1.8 \mu\text{mol}/\text{m}^2\text{-sup}$ and the crushed supports in this study had a maximum adsorption of $0.7 \mu\text{mol}/\text{m}^2$. Using unmodified alumina spheres, it was determined that SEA only occurs as a thin outer shell at low concentrations of platinum (CPA), the depth of this shell ($\sim 0.3 \text{ mm}$) was independent of average pore diameter.

Temperature programmed oxidation (TPO), digestion/ICP, and a series of support wetting experiments were performed to investigate possible contamination and to decouple proton diffusion from metal diffusion and capillary imbibition. TPO indicates that although surface carbon was present it had no measurable effect on the depth of metal adsorption at low concentrations of platinum (CPA). The 36 element ICP analysis indicated significant quantities of Sodium, Nickel, and Zinc, providing a possible explanation for the differences in maximum Pt adsorption. It was concluded that steric hindrance of CPA was the primary factor limiting radial metal penetration, a finding which was supported by the rates of diffusion limited proton exchange. In addition, as the concentration of platinum (CPA) increased, internal metal diffusion increased, while overall metal uptake decreased.

Finally, platinum tetra amine nitrate (PTA) was investigated as an alternative to CPA. Where anionic $[\text{PtCl}_6]^{-2}$ undergoes SEA in the acidic region, the cationic Pt^{+2} species most likely undergoes ion exchange with existing cationic species in the alumina support over a wide range of solution pH. Here metal penetration surpassed the 0.3 mm limit previously mentioned obtaining complete saturation after 7 hours in solution at a low concentration of platinum.

Table of Contents

Abstract	ii
List of Tables	v
List of Figures	vi
Chapter 1: Introduction	1
Chapter 2: Experimental	4
A. Synthesis	4
B. Characterization	6
Chapter 3: Results and Discussion.....	8
A. Catalysis Preparation	8
B. Proton Diffusion.....	13
C. Adsorption and Internal Diffusion of Platinum	16
Chapter 4: Conclusions	25
References.....	26
Appendix A: Aluminas	32
Appendix B: Norit Carbon.....	38

List of Tables

Table 2.1: Physical Properties for Supports analyzed in this study. Note that Alumina A and C have the same total porosity, but C contains macropores.....	4
Table 3.1: Elemental analysis of Alumina A and B, and Norit Carbon. Samples were dissolved in aqua regia and sonicated for 30 minutes. Of the 36 elements analyzed, the 13 listed values reflect 13 signals after subtraction of the aqua regia solution.	14
Table 3.2: Reaction rate constant (k), observed reaction order (α'), and true reaction order (n) of Alumina A, B, and C.	15

List of Figures

- Figure 1.1:** Protonation and deprotonation of supports based on the point of zero charge of the support and the pH of the solution its placed in [7]. 2
- Figure 1.2:** Pore complex-combining the effects of imbibition, external and internal diffusion, and adsorption [10]. 3
- Figure 3.1:** A) Micropore analysis for Norit Carbon. B) Hg Intrusion data for Alumina A, B, and C. Note that A and C have the same surface area but C contains macropores. C) N₂ BJH Data for Alumina A, B, and C. D) Micropore analysis for Alumina A, B, and C. All micropore analyses were fitted using N₂ DFT Model with slit geometry..... 9
- Figure 3.2:** pH shift plots of alumina and carbon using <44 μm powder and formed supports after 1 and 24 hours in solution. All solutions used a surface loading of 10000 m²/L and were agitated for the duration of the experiment..... 11
- Figure 3.3:** Platinum (CPA) uptake survey on <44 μm powder alumina and carbon supports. Data collected by ICP after 1 hour in agitation. Solution conditions: 10000 m²/L surface loading, and a 3400 PPM platinum solution concentration. RPA model data and experimental data collected from Regalbuto [9, 19]. 13
- Figure 3.4:** pH_f kinetics for alumina spheres (top left) and <44 μm fine powder (top right). Proton concentration in solution for alumina spheres (bottom left) and <44 μm fine powder (bottom right) with a metal free solution at an initial pH of 2.6. All experiments used a surface loading of 10000 m²/L with an initial pH of 2.6 (HCl). Dotted lines are added to guide the eye..... 18
- Figure 3.5:** pH_f kinetics (top) and proton concentration in solution (bottom) for alumina A, B and C comparing a metal free solution and a solution containing 200 ppm platinum (CPA)..... 19
- Figure 3.6:** XRF for Alumina A following SEA. Prior to metal addition, the support was modified. 1) Dry support similar to the traditional method of preparation. 2) Support pre wet in DI water. 3) Support pre wet in pH adjusted solution. Results show no significant difference. 21

Figure 3.7: Temperature Programmed Oxidation of Carbon on Alumina A. Sample was ramped from 25°C to 700°C at a ramp rate of 20°C/min in 10% O ₂ Bal Argon (top). XRF for Alumina A following SEA. Prior to metal addition, the support was modified. 1) Dry support similar to the traditional method of preparation. 2) Support calcined at 500°C. 3) Support in vacuum 30 inHg below atmospheric pressure during experiment. Results show no significant difference between pretreatment and experimental methods. This suggests that imbibition and proton diffusion are not limiting the total quantity or metal deposited	22
Figure 3.8: Uptake (top) and XRF (bottom) surveys for Alumina C following SEA at 200, 1000, and 3400 PPM platinum concentrations at a 10% excess monolayer. XRF survey was examined after 48 hours for 200 and 1000 PPM platinum, 24 hours for 3400 PPM platinum.	23
Figure 3.9: XRF for Alumina A following Ion Exchange with Platinum Tetra Ammine Nitrate (PTA), using 200 ppm platinum. Results show that metal diffusion is a function of time with PTA and ion exchange with formed alumina supports.	24
Figure A.1: N ₂ -DFT fits compared with experimental data for alumina A, B, and C. In all cases, the experimental results agree with the selected model	32
Figure A.2: pH shift plots for alumina A, B and C. Comparisons are made between metal free solutions and solutions containing 200 ppm platinum (CPA) for formed spherical supports and 200-325 mesh powder derived from bulk 1mm OD spheres at a 10000 m ² /L surface loading.	33
Figure A.3: Uptake surveys after 48 hours for alumina A, B and C using 200 ppm platinum (CPA) at a surface loading of 10000 m ² /L. Comparisons are made between formed spherical supports and 200-325 mesh powder derived from bulk 1mm OD spheres.....	34
Figure A.4: 200 ppm platinum (CPA) uptake survey, with 10000 m ² /L surface loading, on formed alumina A spheres after 24 hours in solution (Left), and Al concentration leached into the bulk solution under acidic conditions for 24 hours as detected by ICP (Right)	35
Figure A.5: pH _f kinetics (top) and proton concentration in solution (bottom) for alumina A spheres with a metal free solution at an initial pH of 2.6 as a function of mixing speed.....	36

Figure A.6: XRF analysis measuring the counts per second of platinum as a function of distance from the edge of formed support of Alumina A (top), B (middle), and C (bottom) using 200 ppm platinum (CPA)..... 37

Figure B.1: Experimental adsorption isotherm for Norit carbon compared to a slit geometry N₂ adsorption model. The difference between fits suggests good agreement and the absence of mesopores 38

Chapter 1: Introduction

Metallic catalysts today dominant the petrochemical and chemical industries worldwide. The metallic catalysts used today are for selective hydrogenation of olefin streams and pyrolysis gasoline, catalytic reforming, hydrocracking, isomerization of paraffins, auto-exhaust gases, and many more industrial applications. To better understand the exact phenomena of metallic catalyst synthesis, Brunelle in 1978 [1] hypothesized that an oxide in a metal precursor solution away from its point of zero charge (PZC) will have an electrostatic adsorption with the noble metal complex. For decades now, this electrostatic adsorption has been closely studied.

The electric double-layer model of physical adsorption originally proposed by James and Healy in the early seventies [2-4] was later revised by Regalbuto et al resulting in a reduced dependence on assumed chemical interactions for metal adsorption [5]. Further simplifications to the model, known as the revised physical adsorption (RPA) model, have instead been able to accurately predict metal-surface interactions on a variety of support materials based strictly on columbic forces [6] i.e. the net charge after protonation and deprotonation of surface functional groups. Due to these groundbreaking discoveries, the metal-surface interactions on a variety of supports based on columbic forces has been characterized as strong electrostatic adsorption (SEA) [6]. Due to the revised physical adsorption (RPA) model [6], support interactions with precursor metals can be characterized strictly on the point of zero charge of the support and the pH of the metal solution. For a support being placed in a pH metal solution below the point of zero

charge, the surface of the support will become protonated and adsorb anionic metal precursors [7]. In contrast, for a support being placed in a pH metal solution above the point of zero charge, the surface of the support will become deprotonated and adsorb cationic metal precursors [7]. Both scenarios of protonation and deprotonation of supports are illustrated in Figure 1.

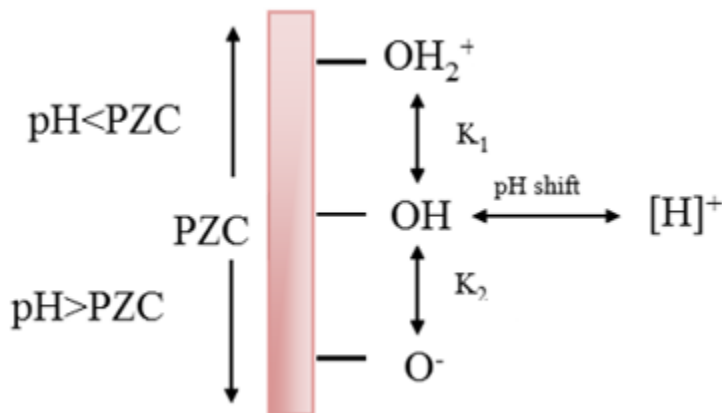


Figure 1.1: Protonation and deprotonation of supports based on the point of zero charge of the support and the pH of the solution its placed in [7].

In many ways the electrostatic adsorption of ligand stabilized transition metal ions can be compared to the processes governing catalytic reactions. In a chemical reactor, the reactants must first migrate through the bulk fluid to access the outer catalytic surface. The remaining unreacted material then enters the carrier pore network, displaces product material and unreacted components, then activates on an available site [8]. In electrostatic adsorption on a formed support, the bulk solution exchanges protons with the outer surface of the support material until coulombic interactions cause metal complex adsorption. At the same time, liquid enters the pore network and displaces trapped air creating a convective force that assist in the transport of additional protons and metal precursor until a surface charge is established and adsorption occurs.

With the point of zero charge being in the basic regime of pH for the aluminas and carbon analyzed, an anionic metal precursor was used to measure the metal adsorption and diffusion [7]. The metal precursor used was chloroplatinic acid (CPA). When using an anionic metal precursor such as CPA, the metal uptake increases as pH decreases, due to there being a stronger charge difference between the support and the metal precursor solution [9].

Up until now, no publication has exclusively examined SEA with formed supports. The current study aims to extend the fundamental understanding of strong electrostatic adsorption to include the processes of external mass transfer limitation, internal mass transfer limitation, adsorption, and the displacement of air by capillary action with a liquid (imbibition) on formed supports, summarized below.

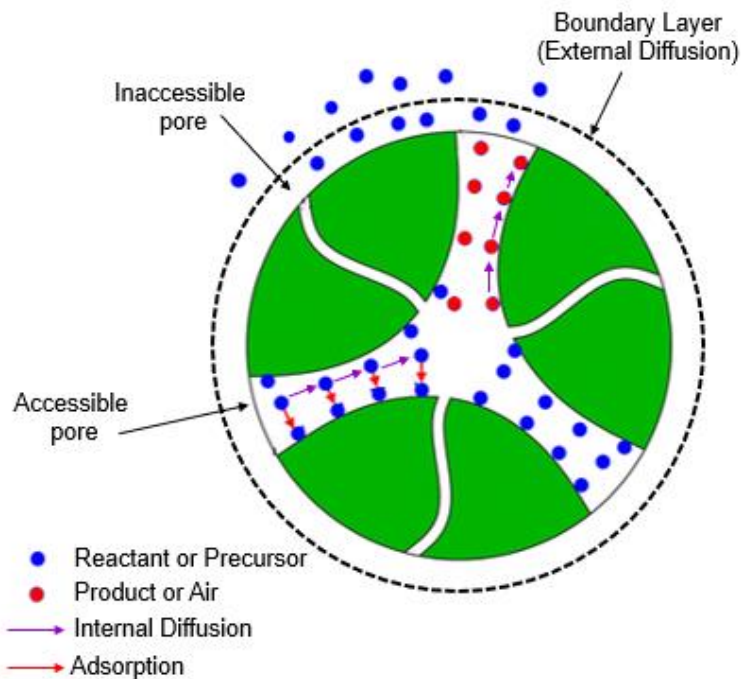


Figure 1.2: Pore complex-combining the effects of imbibition, external and internal diffusion, and adsorption [10].

Chapter 2: Experimental

A. Synthesis

1. Materials

Three alumina materials were provided by BASF and characterized with N₂ BET/BJH, Hg porosimetry, and metal free pH shift profiles for PZC determination, shown in Table 1. N₂ adsorption isotherms of the aluminas are shown in the appendix figures. Norit carbon (1230 m²/g N₂ BET, micromeritics ASAP 2020) was provided by ADM. N₂ adsorption isotherms indicated that the pore structure of the Norit Carbon was strictly microporous, shown in the appendix figures.

Table 2.1: Physical Properties for Supports analyzed in this study. Note that Alumina A and C have the same total porosity, but C contains macropores.

	Shape	Diameter (mm)	Average Pore Diameter (Å)	PZC	Phase	N ₂ BET Surface Area (m ² /g)
Al ₂ O ₃ - A	Sphere	3.3 ± 0.2	Micro (12) Meso (34)	~9.4 ⁽¹⁾	Transitional Alumina	372
Al ₂ O ₃ - B	Sphere	3.3 ± 0.2	Micro (12) Meso (42)	~9.2 ⁽¹⁾	Gamma Alumina	180
Al ₂ O ₃ - C	Sphere	3.4 ± 0.4	Micro (12) Meso (42) Macro (24800)	~9.2 ⁽¹⁾	Transitional Alumina	364
Norit Carbon	Cylinder	0.8 (Diameter) 2.4 ± 0.6 (Length)	Micro (19)	~9.0 ⁽¹⁾	-	1238

2. pH Shift Analysis

pH shift experiments were conducted on formed supports using 20 mL ultrapure water solutions (Surface loading of 10000 m²/g-sup for supports) pH adjusted with HCl or NaOH. Solutions were continuously shaken at 70 RPM on a KJ-201BD Orbital Shaker, and the pH was measured at 1 and 24 hours with an ORION ROSS Ultra Combination pH probe. This procedure was repeated using the same support ground and sieved to a <44 μm mesh powder using a mortar and pedestal. The formed supports and powdered material are denoted as spheres and powder throughout this manuscript. Additional pH shift analysis of alumina supports is displayed in appendix figures.

3. Uptake Surveys

Uptake experiments were conducted on formed Alumina and Norit Carbon supports using 20 mL 3400 ppm chloroplatinic acid solutions (CPA) from Sigma-Aldrich (Surface loading 10000 m²/g-sup) pH adjusted with HCl or NaOH. Solutions were continuously shaken at 70 RPM on a KJ-201BD Orbital Shaker, and the pH was measured at 1, 3, 5, and 7 hrs. This procedure was repeated using the same support ground and sieved to a <44 μm mesh powder using a mortar and pedestal. The formed supports and powdered material are denoted as spheres and powder throughout this manuscript. Additional uptake surveys of alumina supports are displayed in appendix figures.

4. Pre-Wet Versus Dry Support:

Experiments were also conducted to determine the effects of imbibition and proton diffusion on formed supports. The “Pre-Wet” notation indicates that supports were equilibrated in ultrapure water for 24 hours (removal of imbibition) or equilibrated in

ultrapure water pH adjusted to acidic conditions of experiment (removal of proton diffusion). Following equilibration of the formed support, it was lightly dabbed dry before being added to the pH adjusted test solution at a SL of 10000 m²/L-solution. Dry support conditions are denoted as placing the formed support straight into the pH adjusted 20 mL ultrapure solutions.

B. Characterization

1. X-Ray Fluorescence (XRF)

Fischer XDAL X-ray fluorescence (XRF) was used to measure the internal metal diffusion within the formed supports. Following strong electrostatic adsorption, the formed supports were removed from their platinum precursor solutions, vacuum dried for 24 hours in a VWR Vacuum Oven and then reduced in-situ in flowing 50% H₂ balance Ar (800 SCCM) at 200 °C for 4 hours. The formed supports were then sliced in half and examined from one edge of the support to the other and examined using counts per second, which was calibrated using dry impregnation of platinum on the formed alumina supports.

2. ICP Analysis of Metal Adsorption and Digestion of Supports

A PerkinElmer Avio 200 ICP was used to detect platinum uptake and aluminum leaching of the supports. The platinum adsorption experiments measure the micromoles of platinum adsorbed per unit of support surface area. To get an accurate discrepancy among the supports, the same surface loading was used. Since the surface area of each formed support was different, an accurate amount of support mass was obtained and used for experimental studies.

Following each metal containing experiment, ICP was used to determine the PPM (mg/L) of platinum in solution, before and after. The difference between the initial measurement and the measurement of interest is the uptake of metal in terms of mass per unit of support surface area. In addition to platinum being measured for the alumina supports, aluminum concentration was also measured to determine the leaching of support into the metal precursor solution. The aluminum concentration measured for the preliminary studies of alumina dictated which pH would be used.

The metal precursor used for the alumina and carbon supports, chloroplatinic acid (CPA), is known for retaining one hydration sheath [11, 12]. In addition, Regalbuto [9], discovered that at low pH values up to 5, PtCl_6^{2-} ions dominate the solution. Therefore, for the alumina and carbon formed supports, platinum ions with six chlorides attached to it can be assumed throughout.

In addition, the alumina and carbon supports were digested in aqua regia (1 gram per support in 5 mL of aqua regia) and examined using ICP to detect elemental contaminants. This procedure was done using the support ground and sieved to a <44 μm mesh powder using a mortar and pedestal.

3. Temperature Programmed Oxidation:

Temperature Programmed Oxidation (TPO) experiments were conducted on support ground and sieved to a 25-44 mesh powder using a mortar and pedestal. TPO analysis of the sample was ramped from 25°C to 700°C at a ramp rate of 20°C/min in 10% O_2 Bal Argon. Prior to the TPO experiment, temperature programmed desorption (TPD) was investigated to remove any form of carbon dioxide.

Chapter 3: Results and Discussion

A. Catalyst Preparation

The pore structure of Alumina-A was found to be primarily microporous and mesoporous with the same total pore volume as Alumina-C but when analyzed with Hg intrusion, Alumina-C contained a significant number of macropores averaging 5 μm in diameter, Figure 3. Micropore distributions were fit with a slit geometry N_2 -DFT model which was found to be in good agreement with the experimental isotherms, shown in the appendix figures. Using the standard value of 1.25×10^{19} surface “sites”/ m^2 of surface [13], the number of “active sites” for Alumina A, B, and C was calculated to be 4.65×10^{21} , 2.25×10^{21} , and 4.55×10^{21} sites/g-supp suggesting that the rate of pH equilibration should occur much quicker on A and C if the mechanism is limited by the rate of protonation / deprotonation.

However, if the process is limited by mass transport effects Alumina B and C are expected to equilibrate faster compared with Alumina A. In addition, Norit Carbon was examined using nitrogen gas adsorption and it was discovered to be very microporous, and when fit with a slit geometry N_2 adsorption model pore diameters ranged between 10 and 20 Å, as shown in Figure 3. The procedure and methodology used to perform Nitrogen Gas Adsorption and Mercury Intrusion Porosimetry was used from Fan’s publication in 2017 [14].

The Alumina A, B, and C point of zero charge (PZC) was determined using a pH shift experiment of support fine powder (<44 μm) after 1 hour of mixing on the shaker table, shown in Figure 4. Using a high surface loading, in this case 10,000 m^2/g , the PZC was easily obtained due to the rapid proton diffusion between the fine powder surface and

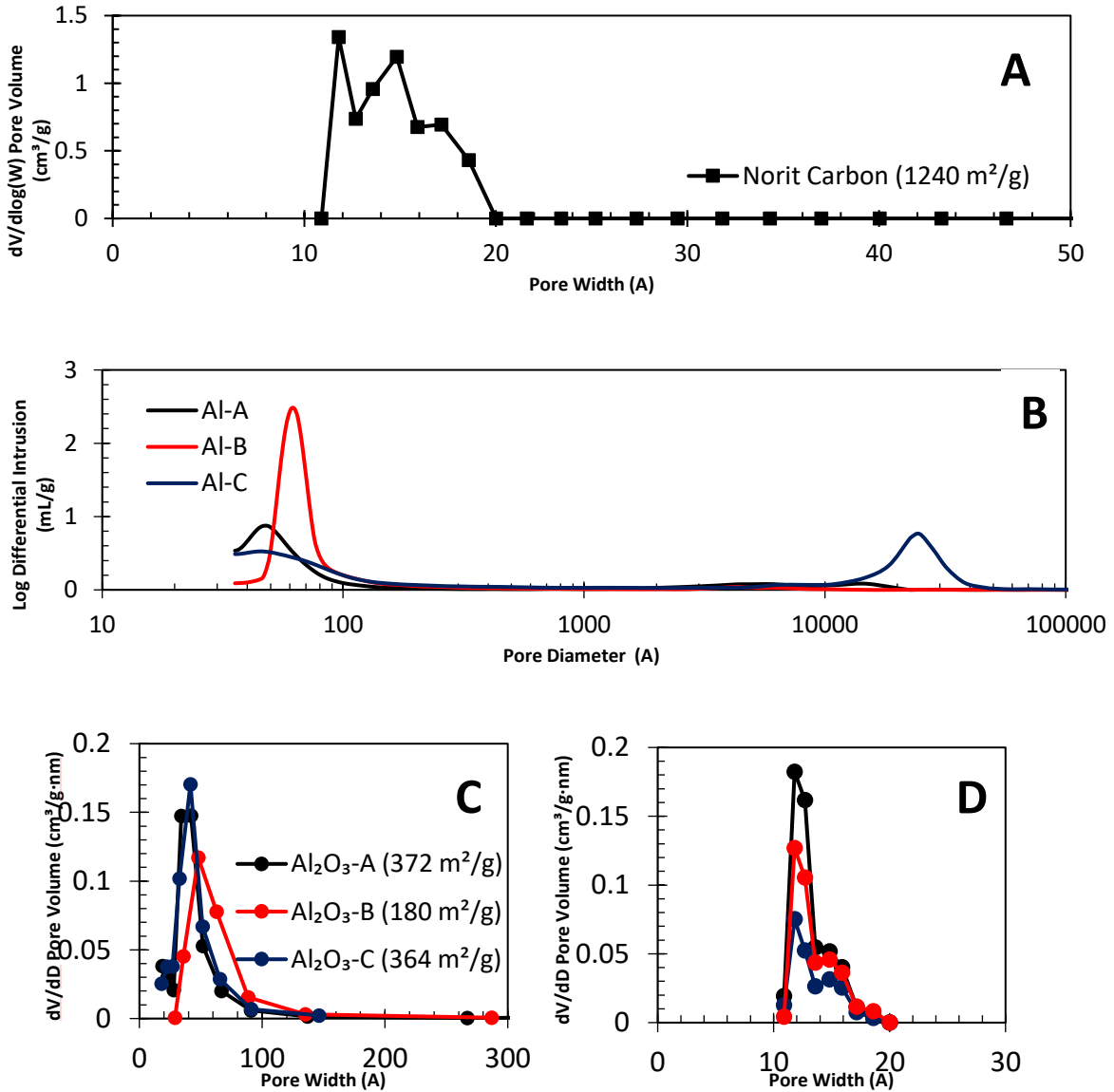


Figure 3.1: A) Micropore analysis for Norit Carbon. B) Hg Intrusion data for Alumina A, B, and C. Note that A and C have the same surface area but C contains macropores. C) N₂ BJH Data for Alumina A, B, and C. D) Micropore analysis for Alumina A, B, and C. All micropore analyses were fitted using N₂ DFT Model with slit geometry.

liquid pH adjusted solution. All three aluminas had PZC's within a range of 0.2 pH units. Although, Alumina A seemed to have a slightly higher PZC than the other two aluminas used for analysis.

In addition, alumina, and carbon pH shift results of the crushed formed support as powder and formed spheres are displayed after 1 and 24 hours, with the powder having much faster proton diffusion than the formed supports. Furthermore, the rate of proton diffusion of formed alumina C has shown to be faster than formed alumina A and B, where alumina C reaches the maximum proton diffusion obtained of its powdered form after 24 hours. A recent article by Jing Li in 2016 [15-18], found that when shale is crushed to about 100 mesh powder or greater, it reduces the proportion of inaccessible pores and increases shale porosity. For the fine powder supports studied below, 325 mesh powder is analyzed, and would, most likely, also increase the number of accessible pores and increase shale porosity as the alumina and carbon supports are crushed to a fine powder. Ultimately, since alumina C has larger pores, this corresponds to less inaccessible pores than the other two formed alumina supports resulting in faster proton diffusion. Platinum uptake surveys for the fine powder carbon and aluminas were then analyzed, displayed in Figure 5. The uptake surveys show that the maximum adsorption takes place between a pH_f of 3 to 4.5 for the aluminas, and between a pH_f of 2 and 3 for the carbon, corresponding to a pH_i range of 2.1 to 2.7. A leaching experiment with ICP was then performed with alumina A spheres, shown in the appendix figures, to detect where aluminum leaching starts to occur with the alumina formed supports, and it was determined that a pH_i of 2.6 was the point where leaching started to accumulate significantly. Therefore, a pH_i of 2.6 was used throughout the remaining experiments to capture the maximum uptake.

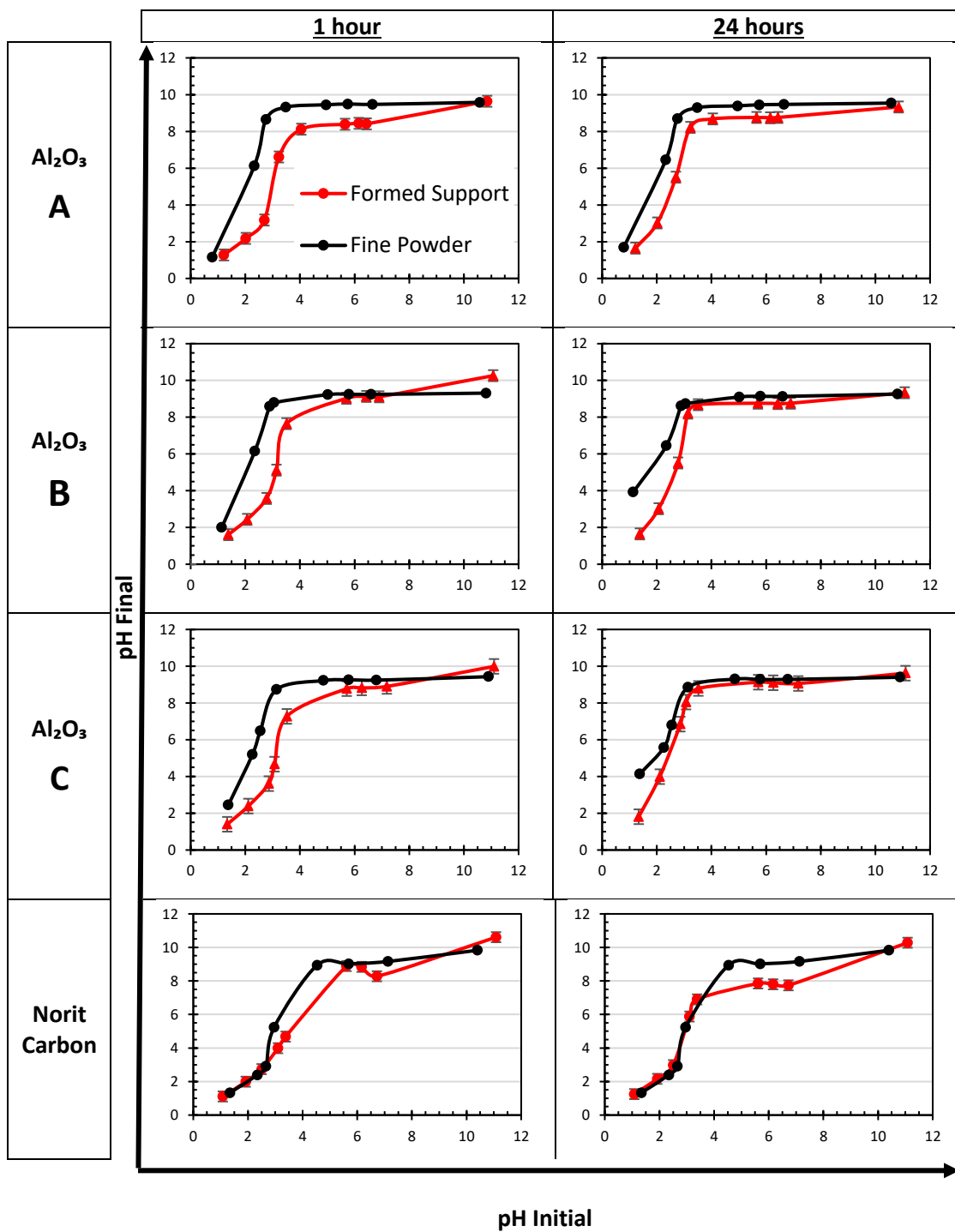


Figure 3.2: pH shift plots of alumina and carbon using <44 μm powder and formed supports after 1 and 24 hours in solution. All solutions used a surface loading of 10000 m^2/L and were agitated for the duration of the experiment.

Regalbuto's previous work [9,12,19], provides insight on how the RPA model and recent experimental data compare to the current supports provided by BASF and ADM. As shown below, the maximum uptake of the formed alumina and carbon supports do not match up to previous supports examined by Regalbuto [9,12,19].

To address the significant difference in uptake between Regalbuto's recent work [9,12,19] and the commercial supports analyzed in the present study, an elemental analysis on two of the aluminas and norit carbon was examined in Table 2. In addition to the commercial supports, a support (SBa200, Sasol, Germany, BET surface area=189 m²/g) used in a previous Regalbuto [12] study, was used for comparison. In this study, 1 gram of fine powder support was placed in 5 mL of aqua regia and sonicated for 30 minutes. After sonicating, the solution was then diluted, filtered, and examined using the ICP. The ICP measured 36 different elements. Although only 13 elements were detected and were sulfur, zinc, phosphorous, cobalt, nickel, barium, iron, silicon, magnesium, manganese, copper, aluminum, sodium, and potassium. Sodium, zinc, and nickel were the highest detected elements, besides aluminum, for the alumina supports. The only significant contaminant on the SBa200 was a small trace of Nickel, with negligible amounts of sodium. In a patent by Riesmeyer [20], he states that in alumina, generally, there is 0.5-0.7% sodium, and provides a viable way of removing the sodium from the alumina supports. In a recent study by McIntosh [21], he found that sodium diffuses into the internal pores of alumina and starts to accumulate, blocking porosity, which ultimately may explain the smaller amount of uptake in comparison to recent studies. In addition, sulfur concentration is very significant on the norit carbon, which may also be restricting metal uptake.

B. Proton Diffusion

After determining the pH initial of interest going forward, mixing conditions were analyzed in appendix figures. In this case study, external mass transfer of protons is analyzed as a function of mixing conditions. In all cases, 20 mL solutions

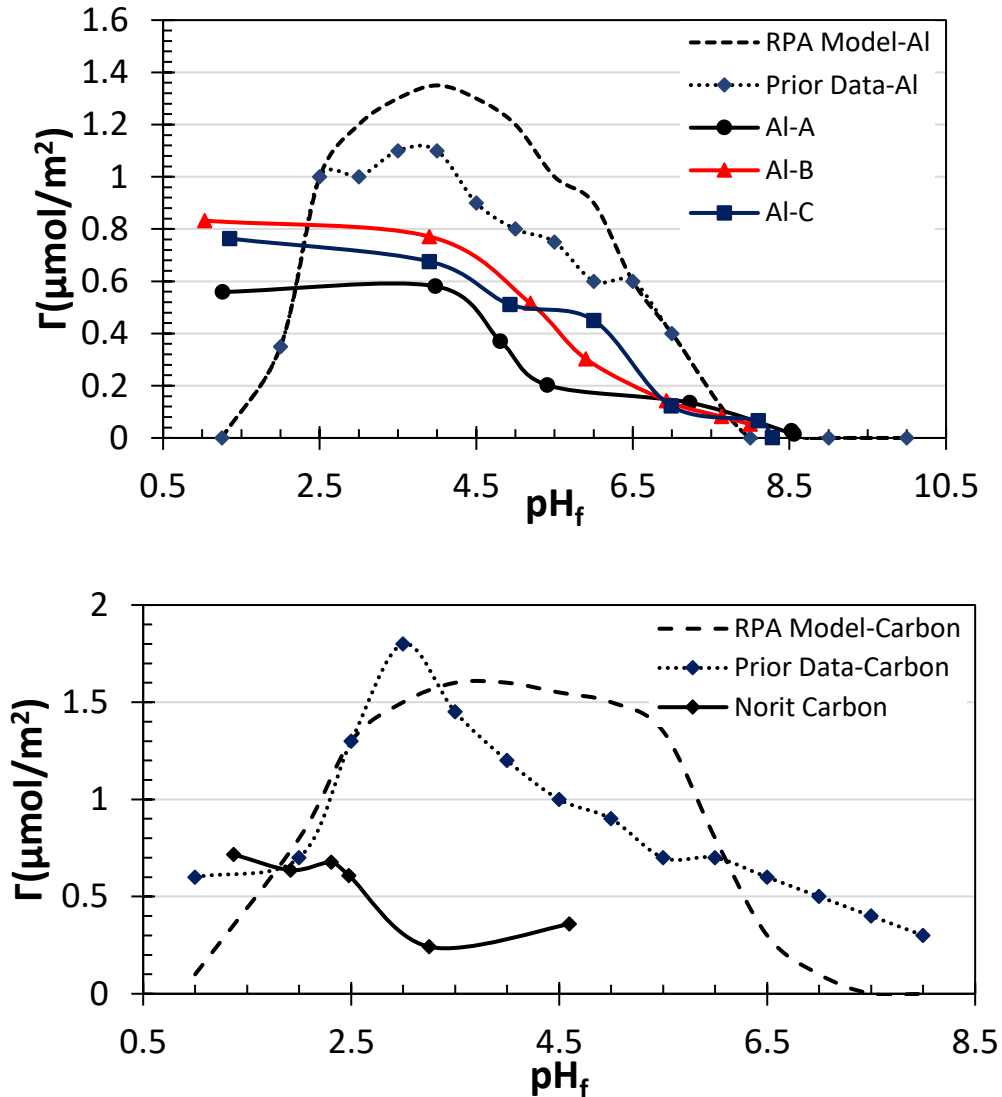


Figure 3.3: Platinum (CPA) uptake survey on $<44 \mu\text{m}$ powder alumina and carbon supports. Data collected by ICP after 1 hour in agitation. Solution conditions: $10000 \text{ m}^2/\text{L}$ surface loading, and a 3400 PPM platinum solution concentration. RPA model data and experimental data collected from Regalbuto [9,12,19].

Table 3.1: Elemental analysis of Alumina A and B, and Norit Carbon. Samples were dissolved in aqua regia and sonicated for 30 minutes. Of the 36 elements analyzed, the 13 listed values reflect 13 signals after subtraction of the aqua regia solution.

Element	Al ₂ O ₃ - A Quantity (PPM)	Al ₂ O ₃ - B Quantity (PPM)	Sasol SBa200 (ppm)	Norit Carbon Quantity (PPM)
1. Sulfur	-	-	-	262.24 ± 0.83
2. Zinc	3.71 ± 0.02	0.30 ± 0.01	0.02 ± 0.01	0.12 ± 0.01
3. Phosphorous	0.41 ± 1.51	1.24 ± 1.46	0.56 ± 0.02	2.57 ± 0.91
4. Cobalt	0.05 ± 0.00	0.02 ± 0.00	-	0.01 ± 0.00
5. Nickle	2.86 ± 0.10	1.71 ± 1.90	2.65 ± 0.09	0.15 ± 0.23
6. Barium	0.02 ± 0.01	0.02 ± 0.01	-	0.16 ± 0.01
7. Iron	0.06 ± 0.00	0.05 ± 0.00	-	0.01 ± 0.00
8. Silicon	0.12 ± 0.00	0.10 ± 0.00	0.04 ± 0.00	0.27 ± 0.00
9. Magnesium	0.50 ± 0.02	0.13 ± 0.01	0.14 ± 0.02	2.54 ± 0.04
10. Manganese	0.26 ± 0.00	0.19 ± 0.00	-	0.25 ± 0.00
11. Copper	0.12 ± 0.00	0.10 ± 0.00	-	0.10 ± 0.00
12. Aluminum	1321.26 ± 6.60	759.32 ± 1.69	527.40 ± 1.44	10.48 ± 0.02
13. Sodium	16.26 ± 0.09	4.97 ± 0.08	0.02 ± 0.02	0 ± 0.00
14. Potassium	-	-	-	5.47 ± 1.19

were prepared using ultrapure water and adjusted to an initial pH (pH_i) of 2.6 using HCl.

As shown in the appendix section, as the stir bar rotations per minute (rpm) increased, the external proton diffusion of the solution onto the alumina surface increased as well.

Although, the mixing table proved to give the greatest rate of external proton diffusion, the mixing speed of the mixing table had little to no effect on the overall external proton diffusion.

Figure 6 addresses the question of proton diffusion on formed supports, comparing transient pH_f data for alumina A, B, and C spheres (left) and powders (right) starting with a pH initial of 2.6. In all cases, 20 mL solutions were prepared using ultrapure water and adjusted to an initial pH (pH_i) of 2.6 using HCl.

Previous work, obtained from Fogler [22] and J.M. Thomas [23], would most likely describe this trend as a profile of a zeroth order reaction. It is assumed that from times 0 to 30 minutes, the proton diffusion with respect to time follow suit of that profile for each formed alumina support. Upon this realization, the slope from time 0 to 30 minutes was used for each alumina support to obtain the reaction rate constant for each alumina support. As shown in Table 3, as the pore size increases, the reaction rate constant increases. Thus, due to the pore geometry alone, proton diffusion is mass transfer limited.

Lastly, the protonation rate is much faster for all three aluminas when comparing powders with a formed support. If an average alumina particle is assumed to be 63 μm in diameter then the total external surface area of the powdered material is $\sim 2700\text{X}$ larger than the same material as a 3.3 mm outer diameter (OD) formed sphere.

Table 3.2: Reaction rate constant (k) of formed Alumina A, B, and C.

	K (L/mol * min)
Alumina A	3.9E-05
Alumina B	4.8E-05
Alumina C	5.9E-05

If the protonation rate is influenced by pore size distribution, as has hypothesized comparing alumina A and C, it is shown that these effects would be eliminated in powdered materials. Additional pH shift plots for Alumina A-C are in the appendix section.

C. Adsorption and Internal Diffusion of Platinum

When 200 ppm CPA is added to solution, the pH profiles follow a similar trend as the metal free solutions with alumina C appearing to approach equilibrium faster than alumina B, and alumina B being faster than alumina A, as shown in Figure 7. In all the additional metal containing cases, 20 mL solutions were prepared using 200 ppm CPA and adjusted to an initial pH (pH_i) of 2.6 using NaOH. Previous efforts have shown that the final pH is determined by the support-solution interaction and is not dependent on the presence of a metal precursor [19]. If the same conclusion holds true when diffusion effects are present than it is likely that the difference in pH_f values for alumina A with and without CPA are due to measurement error.

In addition to adsorption and proton diffusion being analyzed, internal metal diffusion was studied using XRF. Figure 8 shows the counts per second (CPS) versus the distance across alumina A formed spheres. For this study, 60 mL 200 PPM platinum solutions were pH adjusted to a pH_i of 2.6. Upon pH adjustment, the alumina A formed spheres were then added at a surface loading of $580 \text{ m}^2/\text{L}$. After mixing on the mixer table for 7 hours, the alumina spheres were removed, vacuum dried overnight, and then sliced in half using a razorblade. The alumina support was then analyzed with XRF from edge to edge. The alumina A spheres were pretreated in three different ways: traditional strong electrostatic adsorption with dry support (no change), support being pre wetted in ultrapure water solution for 24 hours to eliminate imbibition effects, and support being pre wetted in a pH adjusted ultrapure water solution of 2.6 to eliminate proton diffusion. The distribution of platinum across the spheres was not a function of pore size when analyzed with 200 ppm platinum CPA, as shown in the appendix figures. In addition, there seems to be no

significant difference between pretreatment methods. For each study examined, they were each edge coated by platinum, regardless of proton diffusion or imbibition effects. McIntosh [21], as stated earlier, theorizes that diffusion processes in alumina slowly drive sodium toward the nearest, more thermodynamically stable surfaces. This most likely means that the sodium starts to accumulate in the internal pores and restricts platinum from entering the internal pores of the formed supports, which is, most likely, what is occurring with the formed commercial alumina supports examined. McIntosh [24-27], also discusses how even smaller molecular species such as hydrogen fluoride can lead to pore blocking and since sodium is of similar size, he states that it would have a similar effect on sodium internal pores. Following a close analysis of imbibition and proton diffusion effects on platinum internal diffusion, two additional studies were examined with 200 PPM platinum (CPA). Temperature programmed oxidation was used to measure carbon oxidation with respect to temperature. As shown in Figure 9, the temperature carbon would most likely calcine off at would be about 500°C. Therefore, following the same exact procedure used for XRF in the previous figure, the three studies inspected were: traditional strong electrostatic adsorption with dry support (no change), calcination of the formed alumina support at 500°C, and conducting strong electrostatic adsorption in a vacuum rotovap at 30 inHg below atmospheric pressure. Essentially, the results still exhibit the same story, internal metal diffusion is still limited to the outside ring of the spheres, where it is completely edge coated by platinum. Therefore, regardless of proton diffusion, imbibition, calcination, and wetting effects, platinum internal diffusion ceases to occur after 7 hours using a 200 ppm platinum solution (CPA).

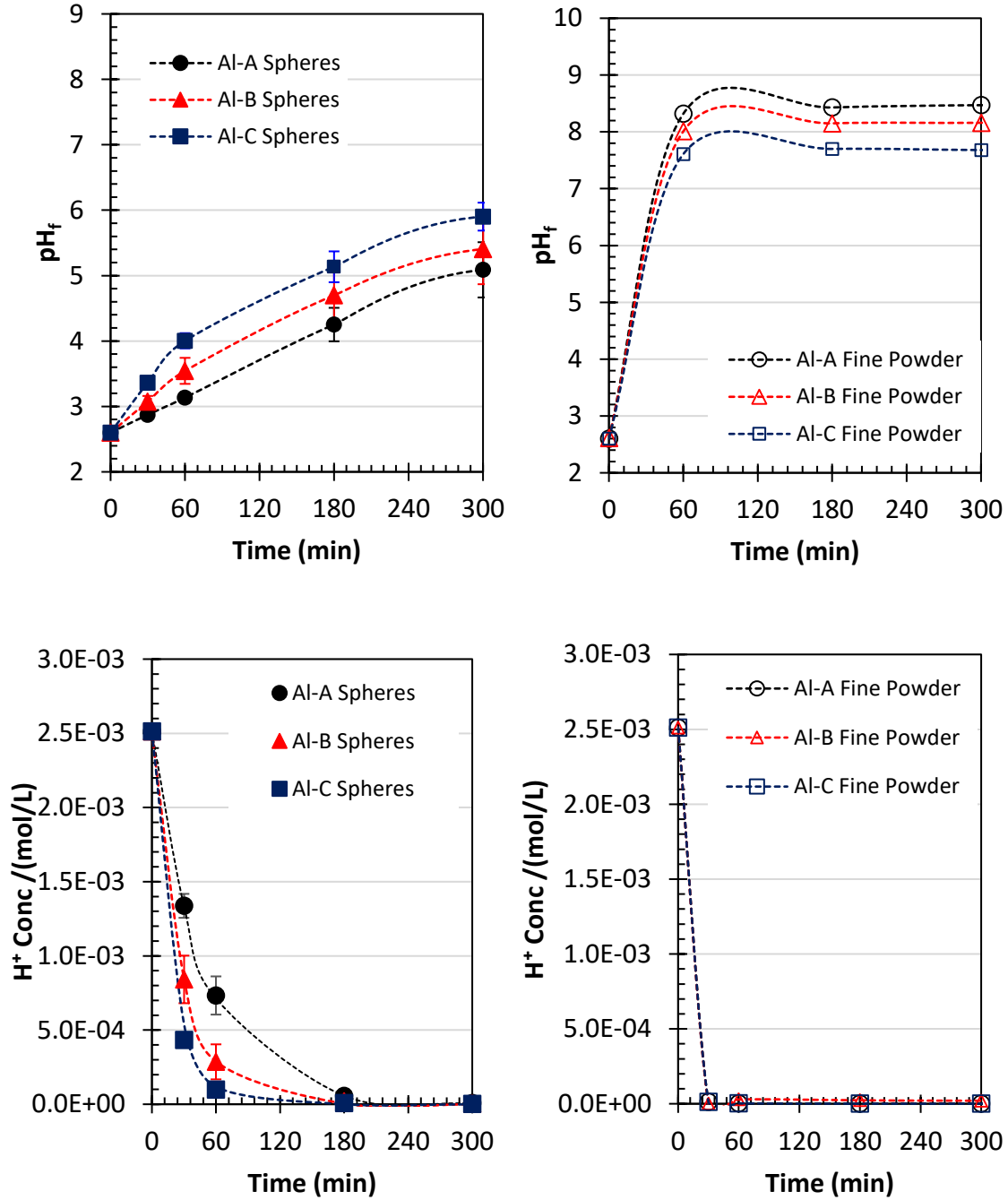


Figure 3.4: pH_f kinetics for alumina spheres (top left) and <44 μm fine powder (top right). Proton concentration in solution for alumina spheres (bottom left) and <44 μm fine powder (bottom right) with a metal free solution at an initial pH of 2.6. All experiments used a surface loading of 10000 m^2/L with an initial pH of 2.6 (HCl). Dotted lines are added to guide the eye.

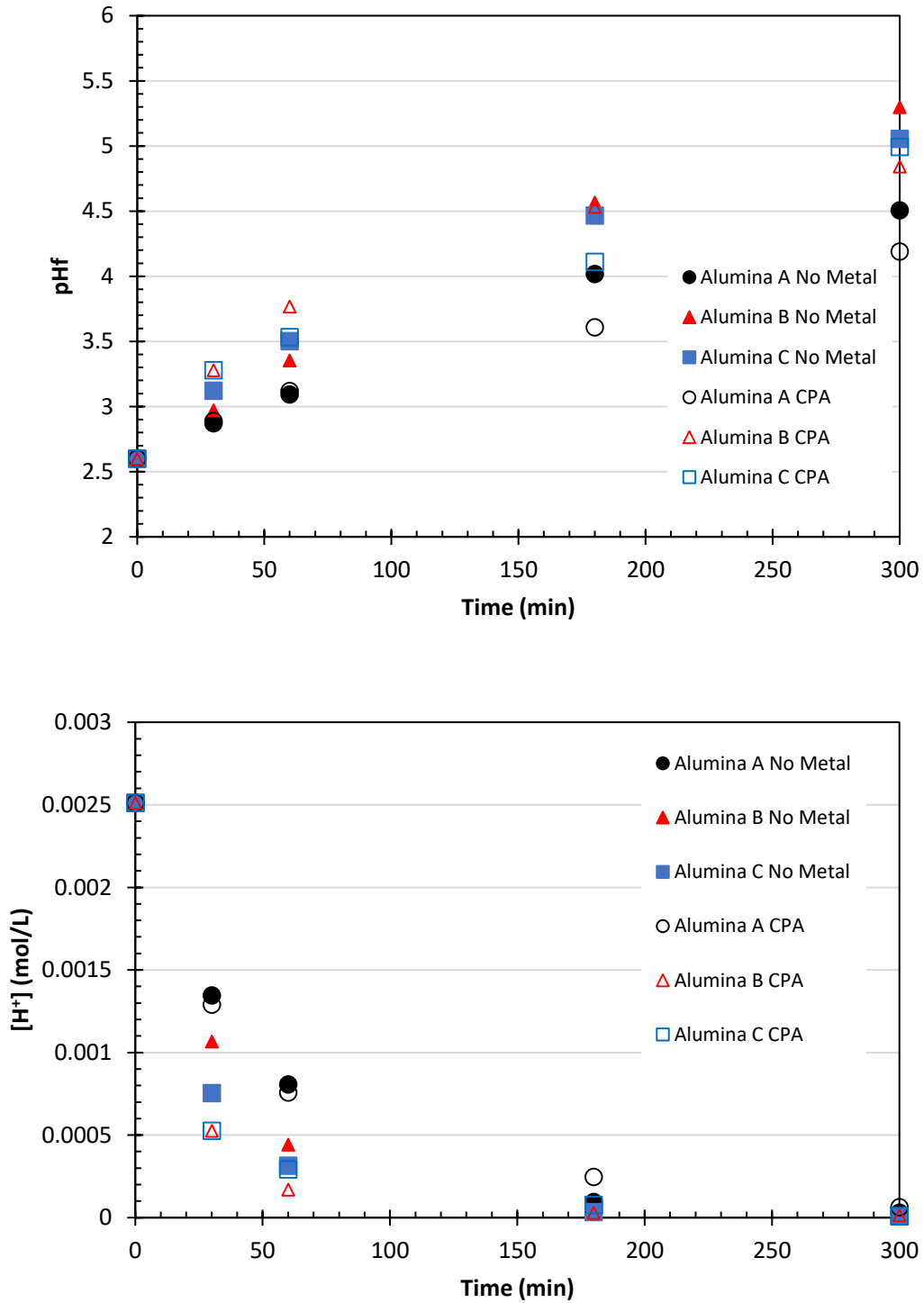


Figure 3.5: pH_f kinetics (top) and proton concentration in solution (bottom) for alumina A, B and C comparing a metal free solution and a solution containing 200 ppm platinum (CPA).

Next, differing concentrations of platinum (CPA) solutions were analyzed with XRF and ICP using alumina C formed support, as shown in Figure 10. The concentrations investigated were 200, 1000, and 3400 ppm platinum. As concentration of platinum increases, internal metal concentration increases. Due to Fick's Law of Diffusion [32], the concentration gradient of the platinum increases as concentration increases. Therefore, internal diffusion will have a stronger driving force to penetrate the internal pores of the alumina C formed support. Although, as concentration of metal increases, platinum uptake decreases. This is most likely due to ionic strength increasing as concentration of platinum increases, which ultimately lowers the amount of platinum uptake, displayed in a recent article by Samad [12]. The article also states how the addition of metal to the solution also might increase the concentration of counterions, which is most likely what is hindering platinum uptake [12]. Hence, as internal metal diffusion increases, uptake of platinum decreases on formed alumina supports.

Lastly, alumina A was investigated using platinum tetra ammine nitrate (PTA), with the same experimental conditions as Figures 8 and 9, shown in Figure 11. As time increases, the internal metal diffusion increases with a 200 PPM platinum solution (platinum tetra ammine nitrate). Previous work has been analyzed using silica with PTA to confirm that the mechanism taking place is indeed ion exchange [28-31]. Although, Regalbuto [11], concluded later that the mechanism is most likely strong electrostatic adsorption. Overall, the mechanism has not been confirmed to be strong electrostatic adsorption or ion exchange with the alumina A support. In the study done by Regalbuto [11], the PZC of the silica was in the acidic regime, thus, giving enough charge to have SEA take place. In contrast, with the alumina A support, the experiment takes place in the

basic regime, which is most likely too close to the PZC to have a significant amount of electrostatic attraction between the metal precursor and the alumina support. Due to the support PZC being at a pH of 9, the mechanism taking place is most likely ion exchange.

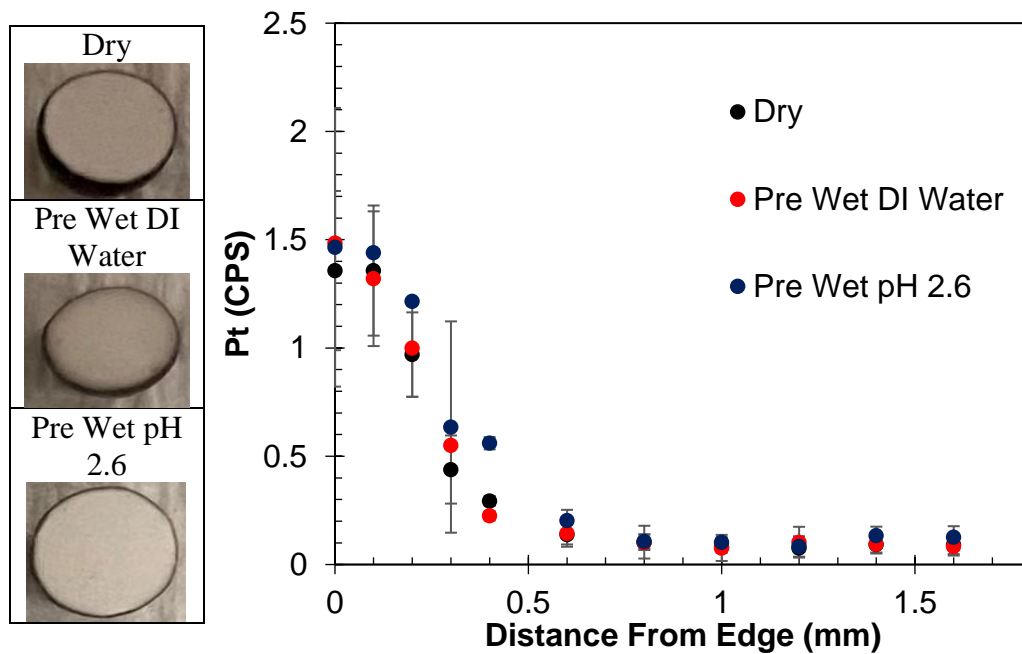


Figure 3.6: XRF for Alumina A following SEA. Prior to metal addition, the support was modified. 1) Dry support similar to the traditional method of preparation. 2) Support pre wet in DI water. 3) Support pre wet in pH adjusted solution. Results show no significant difference.

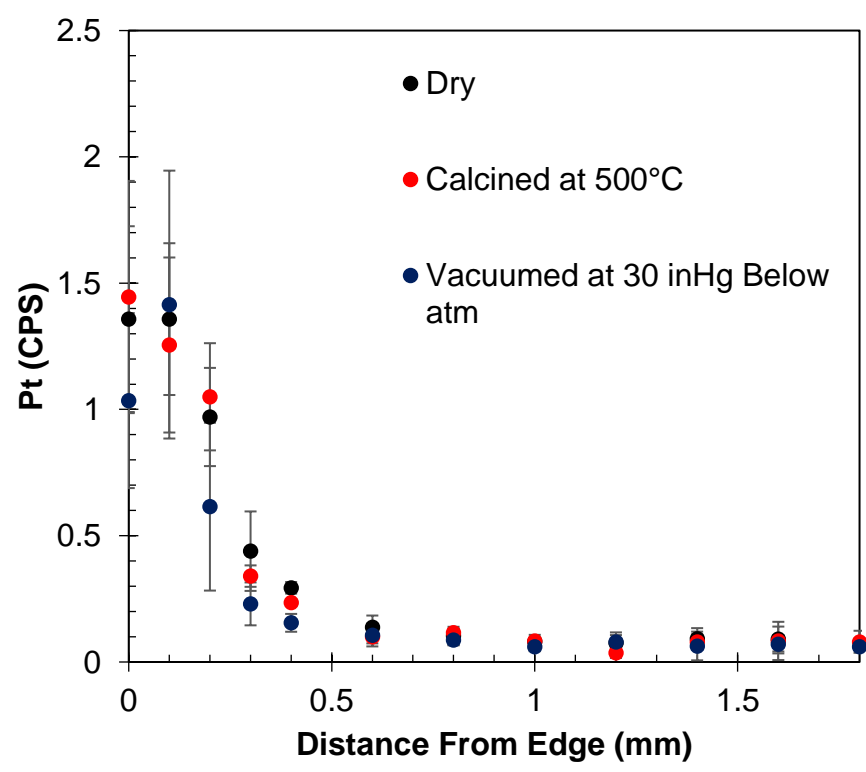
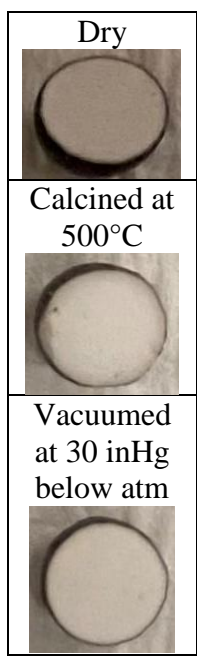
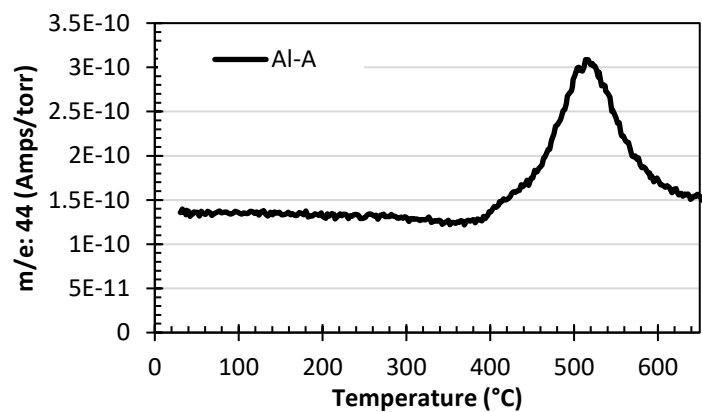


Figure 3.7: Temperature Programmed Oxidation of Carbon on Alumina A. Sample was ramped from 25°C to 700°C at a ramp rate of 20°C/min in 10% O₂ Bal Argon (top). XRF for Alumina A following SEA. Prior to metal addition, the support was modified. 1) Dry support similar to the traditional method of preparation. 2) Support calcined at 500°C. 3) Support in vacuum 30 inHg below atmospheric pressure during experiment. Results show no significant difference between pretreatment and experimental methods. This suggests that imbibition and proton diffusion are not limiting the total quantity or metal deposited.

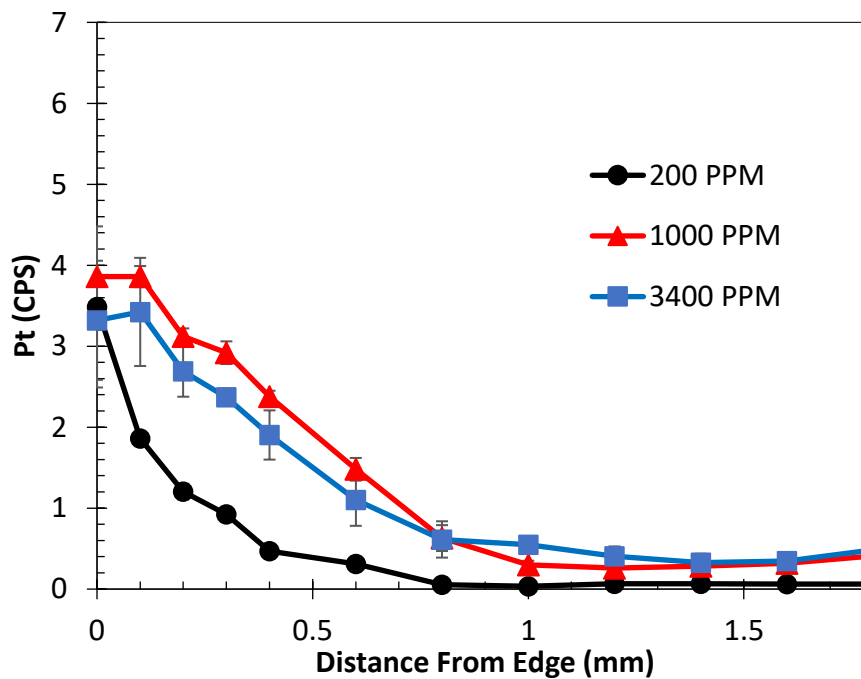
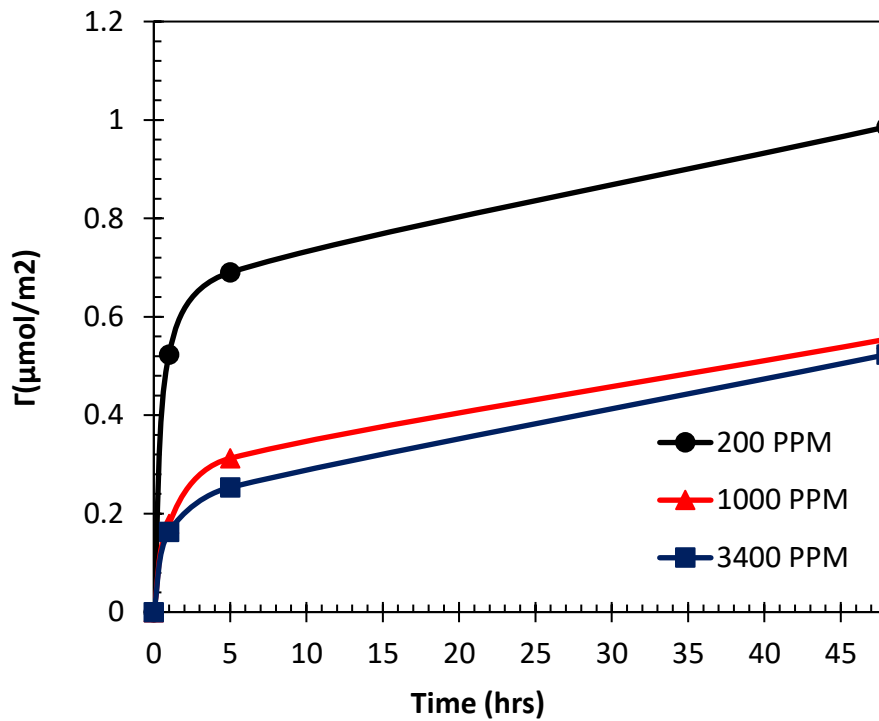


Figure 3.8: Uptake (top) and XRF (bottom) surveys for Alumina C following SEA at 200, 1000, and 3400 PPM platinum concentrations at a 10% excess monolayer. XRF survey was examined after 48 hours.

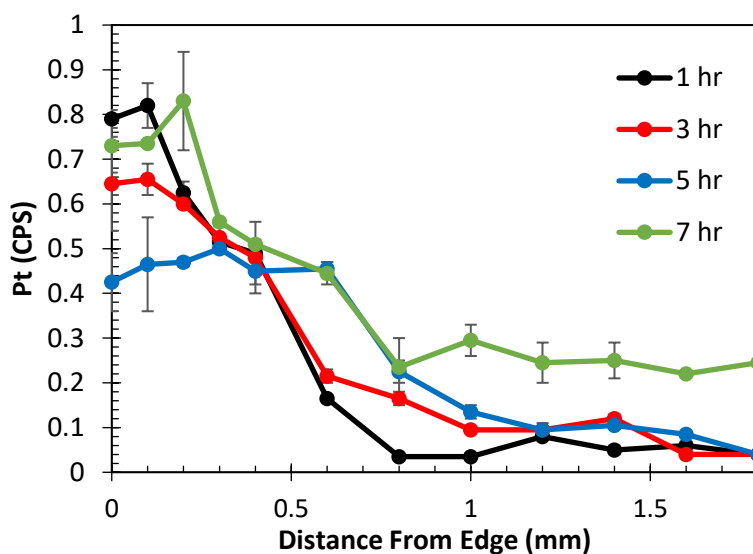
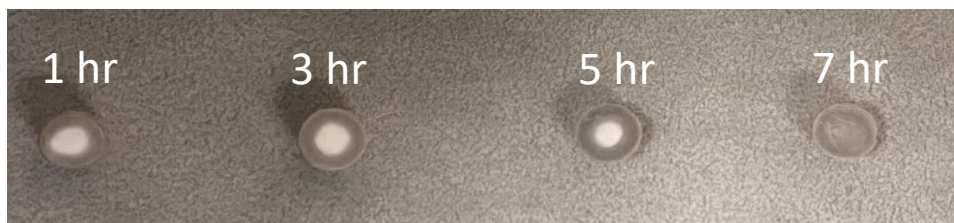


Figure 3.9: XRF for Alumina A following Ion Exchange with Platinum Tetra Ammine Nitrate (PTA), using 200 ppm platinum. Results show that metal diffusion is a function of time with PTA and ion exchange with formed alumina supports.

Chapter 4: Conclusions

Proton diffusion on formed supports has shown to be a function of pore complex. As the pore size of formed alumina supports increases, proton diffusion increases, thus indicating a mass transfer limitation for formed extrudates, while powdered supports have instantaneous proton diffusion. XRF analysis also suggests that imbibition, proton diffusion, wetting, and calcination have negligible effects on internal metal diffusion with CPA at short time studies with low concentration. Elemental ICP analysis suggests detectable amounts of sodium, zinc, and nickel, on the aluminas, as well as sulfur on the norit carbon. Internal platinum diffusion with CPA on formed alumina supports increases as concentration of platinum increases. Consequently, as concentration of platinum increases (CPA), the overall uptake of platinum on formed alumina supports decreases. Lastly, platinum tetra ammine nitrate (PTA) has shown to be a viable precursor option that penetrates the internal pores of alumina at low concentrations of platinum.

References

- [1] Brunelle, J. P. "Preparation of Catalysts by Metallic Complex Adsorption on Mineral Oxides." *Pure and Applied Chemistry* 50, no. 9-10 (1978): 1211–29.
<https://doi.org/10.1351/pac197850091211>.
- [2] James, Robert O, and Thomas W Healy. "Adsorption of Hydrolyzable Metal Ions at the Oxide—Water Interface. I. Co(II) Adsorption on SiO₂ and TiO₂ as Model Systems." *Journal of Colloid and Interface Science* 40, no. 1 (1972): 42–52.
[https://doi.org/10.1016/0021-9797\(72\)90172-5](https://doi.org/10.1016/0021-9797(72)90172-5).
- [3] James, Robert O, and Thomas W Healy. "Adsorption of Hydrolyzable Metal Ions at the Oxide—Water Interface. II. Charge Reversal of SiO₂ and TiO₂ Colloids by Adsorbed Co(II), La(III), and Th(IV) as Model Systems." *Journal of Colloid and Interface Science* 40, no. 1 (1972): 53–64. [https://doi.org/10.1016/0021-9797\(72\)90173-7](https://doi.org/10.1016/0021-9797(72)90173-7).
- [4] James, Robert O, and Thomas W Healy. "Adsorption of Hydrolyzable Metal Ions at the Oxide—Water Interface. III. A Thermodynamic Model of Adsorption." *Journal of Colloid and Interface Science* 40, no. 1 (1972): 65–81.
[https://doi.org/10.1016/0021-9797\(72\)90174-9](https://doi.org/10.1016/0021-9797(72)90174-9).

- [5] Agashe, Krishna B., and John R. Regalbuto. “A Revised Physical Theory for Adsorption of Metal Complexes at Oxide Surfaces.” *Journal of Colloid and Interface Science* 185, no. 1 (1997): 174–89.
<https://doi.org/10.1006/jcis.1996.4493>.
- [6] Hao, X., W.A. Spieker, and J.R. Regalbuto. “A Further Simplification of the Revised Physical Adsorption (RPA) Model.” *Journal of Colloid and Interface Science* 267, no. 2 (2003): 259–64. [https://doi.org/10.1016/s0021-9797\(03\)00644-1](https://doi.org/10.1016/s0021-9797(03)00644-1).
- [7] Regalbuto, John. “Strong Electrostatic Adsorption of Metals onto Catalyst Supports.” *Catalyst Preparation*, 2006, 297–318.
<https://doi.org/10.1201/9781420006506.ch13>.
- [8] Bartholomew, Calvin H., and Robert J. Farrauto. *Fundamentals of Industrial Catalytic Processes*. Hoboken, NJ: Wiley-Interscience, 2006.
- [9] Regalbuto, J.R., A. Navada, S. Shadid, M.L. Bricker, and Q. Chen. “An Experimental Verification of the Physical Nature of Pt Adsorption onto Alumina.” *Journal of Catalysis* 184, no. 2 (1999): 335–48. <https://doi.org/10.1006/jcat.1999.2471>.
- [10] Zhang, Haiyan, Longjian Chen, Minsheng Lu, Junbao Li, and Lujia Han. “A Novel Film–Pore–Surface Diffusion Model to Explain the Enhanced Enzyme Adsorption of Corn Stover Pretreated by Ultrafine Grinding.” *Biotechnology for Biofuels* 9, no. 1 (2016). <https://doi.org/10.1186/s13068-016-0602-2>.

- [11] Schreier, M. “A Fundamental Study of Pt Tetraammine Impregnation of silica1. The Electrostatic Nature of Platinum Adsorption.” *Journal of Catalysis* 225, no. 1 (2004): 190–202. <https://doi.org/10.1016/j.jcat.2004.03.034>.
- [12] Samad, Jadid E., Sean Hoenig, and John R. Regalbuto. “Synthesis of Platinum Catalysts over Thick Slurries of Oxide Supports by Strong Electrostatic Adsorption.” *ChemCatChem* 7, no. 21 (2015): 3460–63. <https://doi.org/10.1002/cctc.201500595>.
- [13] Anderson, John Robert. *Structure of Metallic Catalysts*. London: Acad. Pr, 1975.
- [14] Fu, Feng, and Mizi Fan. *Advanced High Strength Natural Fibre Composites in Construction*. Elsevier Science, 2017.
- [15] Li, Jing, Shixin Zhou, Deliang Fu, Yuanju Li, Yu Ma, Yanan Yang, and Chengcheng Li. “Changes in the Pore Characteristics of Shale during Comminution.” *Energy Exploration & Exploitation* 34, no. 5 (2016): 676–88. <https://doi.org/10.1177/0144598716656064>.
- [16] Hodson, Mark Edward. “Micropore Surface Area Variation with Grain Size in Unweathered Alkali Feldspars: Implications for Surface Roughness and Dissolution Studies.” *Geochimica et Cosmochimica Acta* 62, no. 21-22 (1998): 3429–35. [https://doi.org/10.1016/s0016-7037\(98\)00244-0](https://doi.org/10.1016/s0016-7037(98)00244-0).

- [17] Chen, Yanyan, Lin Wei, Maria Mastalerz, and Arndt Schimmelmann. “The Effect of Analytical Particle Size on Gas Adsorption Porosimetry of Shale.” *International Journal of Coal Geology* 138 (2015): 103–12. <https://doi.org/10.1016/j.coal.2014.12.012>.
- [18] Kuila, Utpalendu, and Manika Prasad. “Application of Nitrogen Gas-Adsorption Technique for Characterization of Pore Structure of Mudrocks.” *The Leading Edge* 32, no. 12 (2013): 1478–85. <https://doi.org/10.1190/tle32121478.1>.
- [19] Hao, X., S. Barnes, and J.R. Regalbutto. “A Fundamental Study of Pt Impregnation of Carbon: Adsorption Equilibrium and Particle Synthesis.” *Journal of Catalysis* 279, no. 1 (2011): 48–65. <https://doi.org/10.1016/j.jcat.2010.12.021>.
- [20] Riesmeyer, August H. REMOVING SODIUM FROM ALUMINA, issued November 26, 1946.
- [21] McIntosh, Grant J., Hasini Wijayaratne, Gordon E. Agbenyegah, Margaret M. Hyland, and James B. Metson. “Impacts of Sodium on Alumina Quality and Consequences for Current Efficiency.” *The Minerals, Metals & Materials Series*, 2018, 533–39. https://doi.org/10.1007/978-3-319-72284-9_70.
- [22] Fogler, H. Scott. *Elements of Chemical Reaction Engineering*. Harlow: Pearson Education, 2016.
- [23] Thomas, John M., and William J. Thomas. *Introduction to the Principles of Heterogeneous Catalysis*. London: Acad. Pr, 1975.

- [24] McIntosh, Grant J., Gordon E. Agbenyegah, Margaret M. Hyland, and James B. Metson. "The Pivotal Role of Alumina Pore Structure in HF Capture and Fluoride Return in Aluminum Reduction." *JOM* 68, no. 9 (2016): 2463–71. <https://doi.org/10.1007/s11837-016-2004-0>.
- [25] McIntosh, Grant J., James B. Metson, Thomas Niesenhaus, Till Reek, and Linus Perander. "Smelter Fluoride Balances: The Interplay Between Alumina Phases, Pore Size Distributions, and the Impacts of Weather." *JOM* 66, no. 11 (2014): 2272–81. <https://doi.org/10.1007/s11837-014-1189-3>.
- [26] McIntosh, Grant J., Gordon E. Agbenyegah, Margaret M. Hyland, and James B. Metson. "Adsorptive Capacity and Evolution of the Pore Structure of Alumina on Reaction with Gaseous Hydrogen Fluoride." *Langmuir* 31, no. 19 (2015): 5387–97. <https://doi.org/10.1021/acs.langmuir.5b00664>.
- [27] Agbenyegah, Gordon E., Grant J. McIntosh, Margaret H. Hyland, and James B. Metson. "Assessing the Role of Smelter Grade Alumina Porosity in the HF Scrubbing Mechanism." *Light Metals 2016*, 2016, 521–25. https://doi.org/10.1007/978-3-319-48251-4_86.
- [28] Goguet, A., M. Aouine, F.J. Cadete Santos Aires, A. De Mallmann, D. Schweich, and J.P. Candy. "Preparation of a Pt/SiO₂ Catalyst." *Journal of Catalysis* 209, no. 1 (2002): 135–44. <https://doi.org/10.1006/jcat.2002.3616>.

- [29] Morrow, B. A., and A. J. McFarlan. “Infrared and Gravimetric Study of an Aerosil and a Precipitated Silica Using Chemical and Hydrogen/Deuterium Exchange Probes.” *Langmuir* 7, no. 8 (1991): 1695–1701.
<https://doi.org/10.1021/la00056a022>.
- [30] Gonzalez, Richard D., and Hiroshi Miura. “Preparation of SiO₂-and Al₂O₃-Supported Clusters of Pt Group Metals.” *Catalysis Reviews* 36, no. 1 (1994): 145–77. <https://doi.org/10.1080/01614949408013923>.
- [31] Zou, Weiqing, and Richard D Gonzalez. “Pretreatment Chemistry in the Preparation of Silica-Supported Pt, Ru, and Pt-Ru Catalysts: An in Situ UV Diffuse Reflectance Study.” *Journal of Catalysis* 133, no. 1 (1992): 202–19.
[https://doi.org/10.1016/0021-9517\(92\)90198-q](https://doi.org/10.1016/0021-9517(92)90198-q).
- [32] Milligen, B Ph, P D Bons, B A Carreras, and R Sánchez. “On the Applicability of Fick's Law to Diffusion in Inhomogeneous Systems.” *European Journal of Physics* 26, no. 5 (2005): 913–25. <https://doi.org/10.1088/0143-0807/26/5/023>.

Appendix A: Aluminas

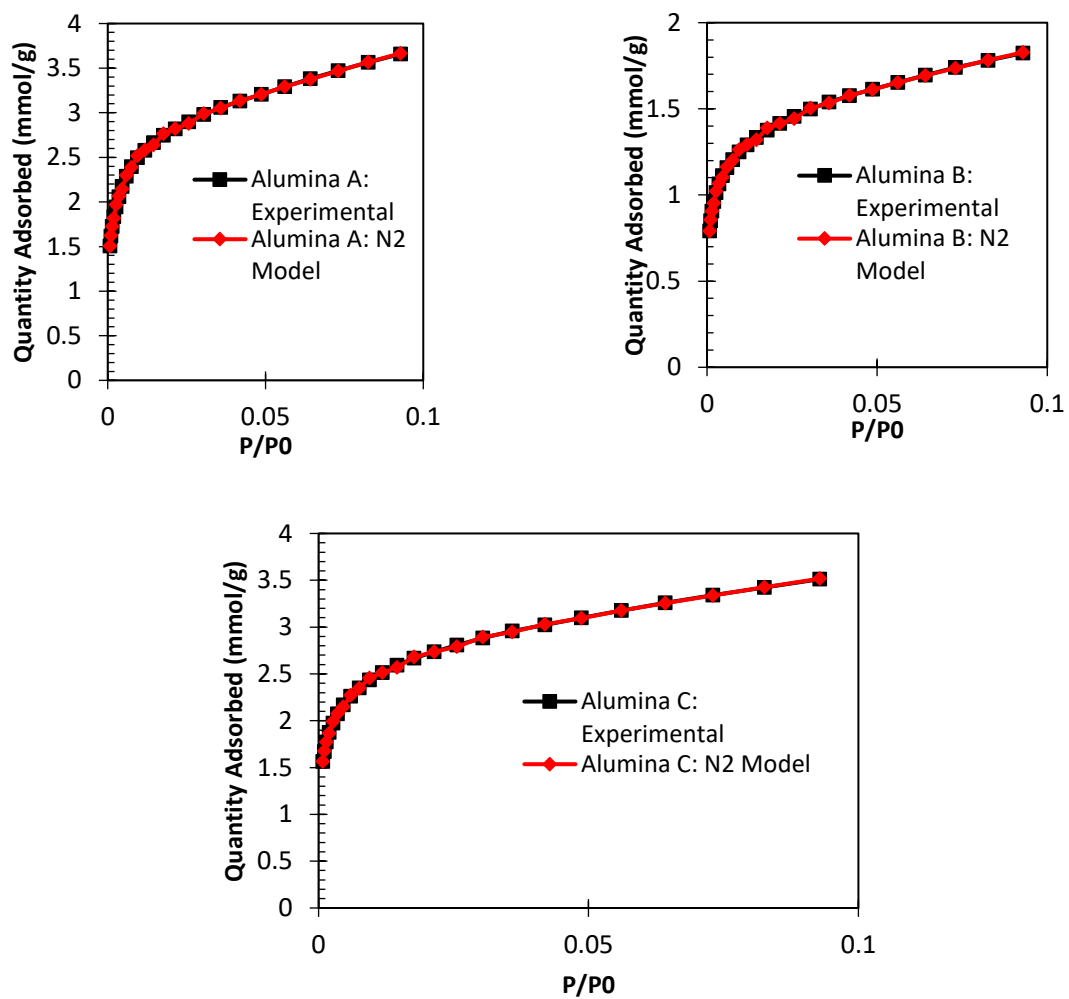


Figure A.1: N₂-DFT fits compared with experimental data for alumina A, B, and C. In all cases, the experimental results agree with the selected model.

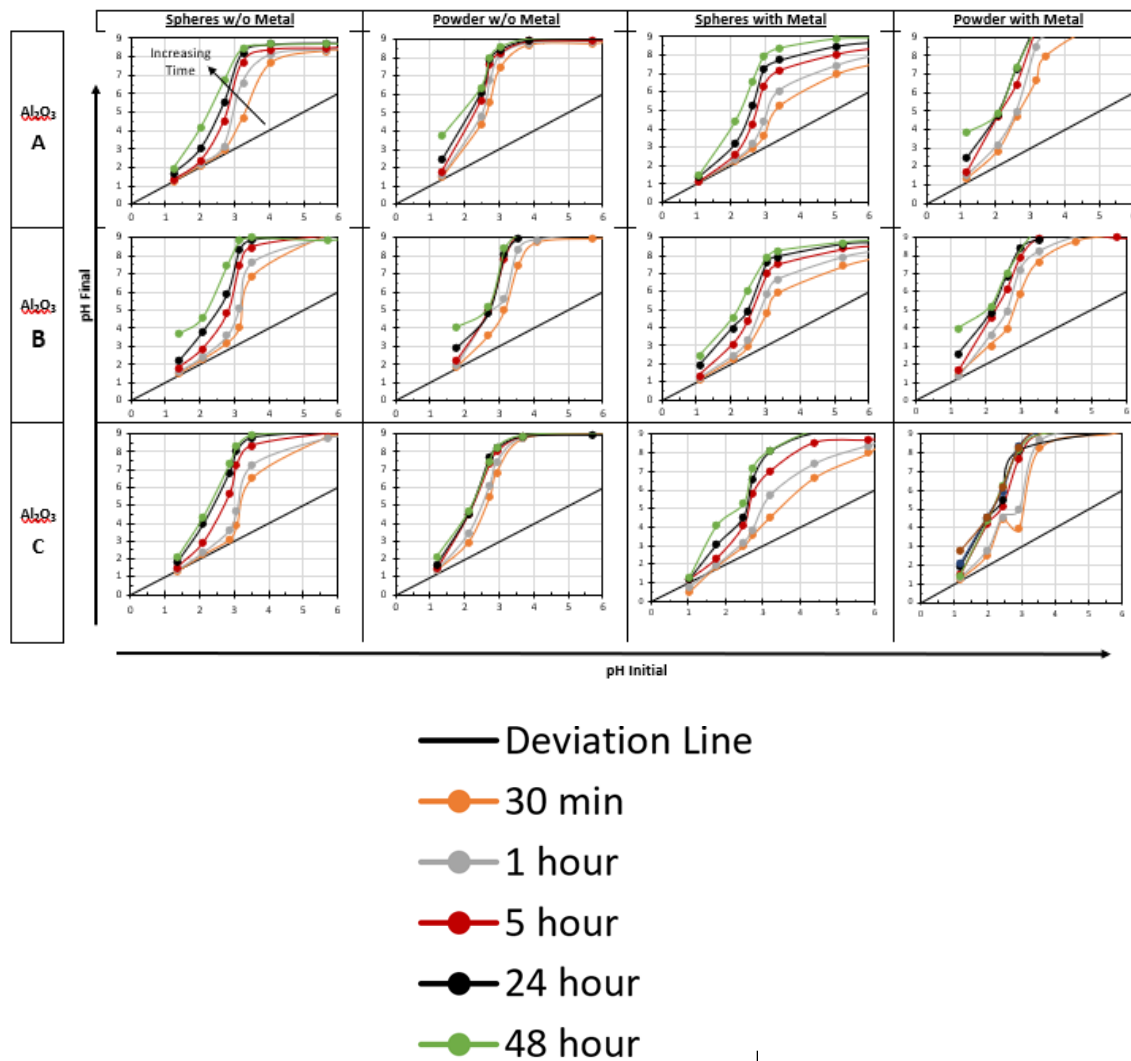


Figure A.2: pH shift plots for alumina A, B and C. Comparisons are made between metal free solutions and solutions containing 200 ppm platinum (CPA) for formed spherical supports and 200-325 mesh powder derived from bulk 1mm OD spheres at a 10000 m²/L surface loading.

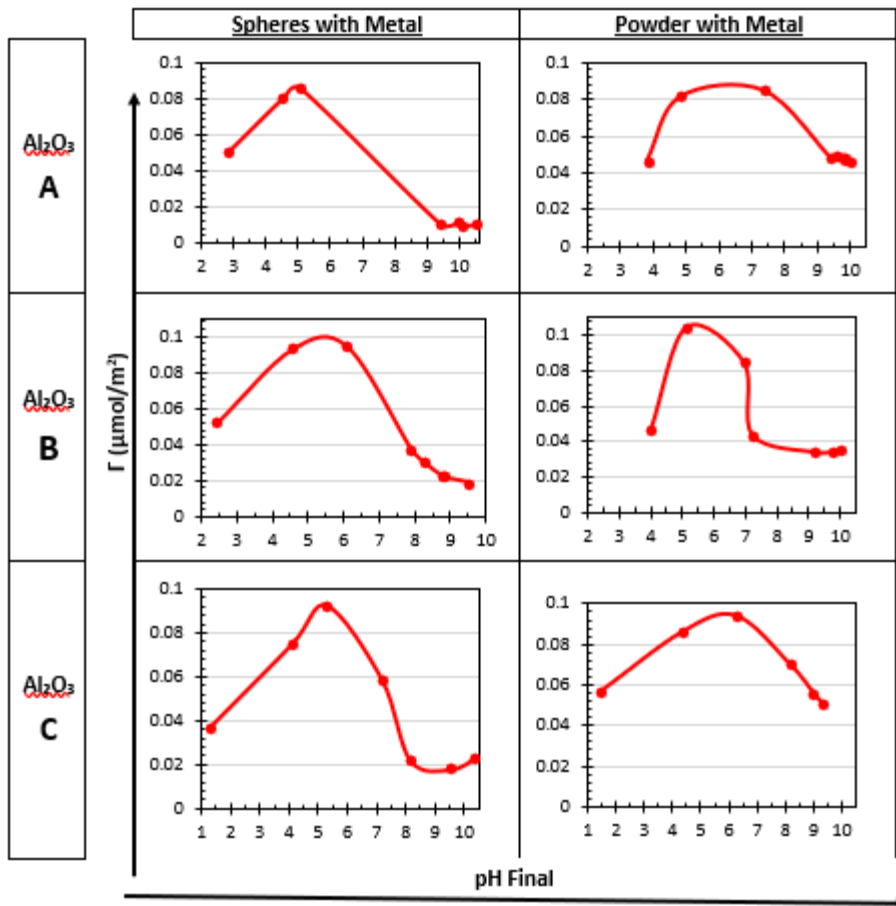


Figure A.3: Uptake surveys after 48 hours for alumina A, B and C using 200 ppm platinum (CPA) at a surface loading of 10000 m²/L. Comparisons are made between formed spherical supports and 200-325 mesh powder derived from bulk 1mm OD spheres.

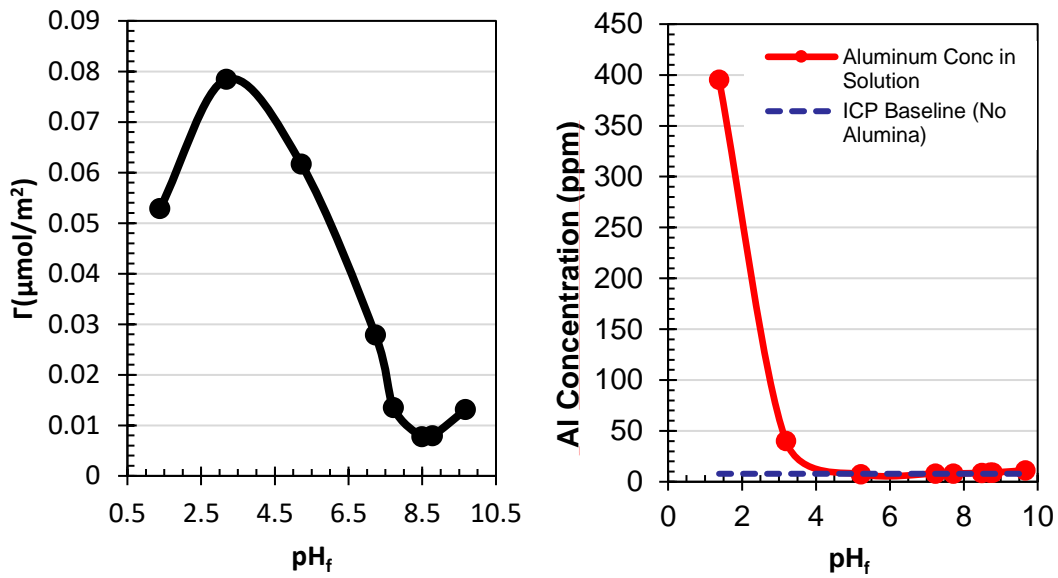


Figure A.4: 200 ppm platinum (CPA) uptake survey, with 10000 m^2/L surface loading, on formed alumina A spheres after 24 hours in solution (Left), and Al concentration leached into the bulk solution under acidic conditions for 24 hours as detected by ICP (Right).

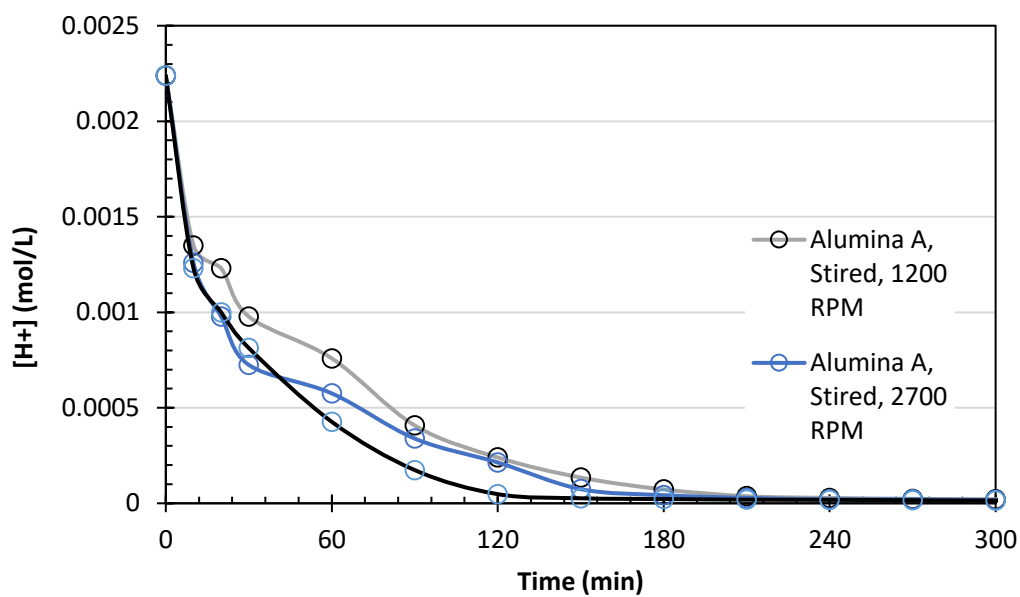
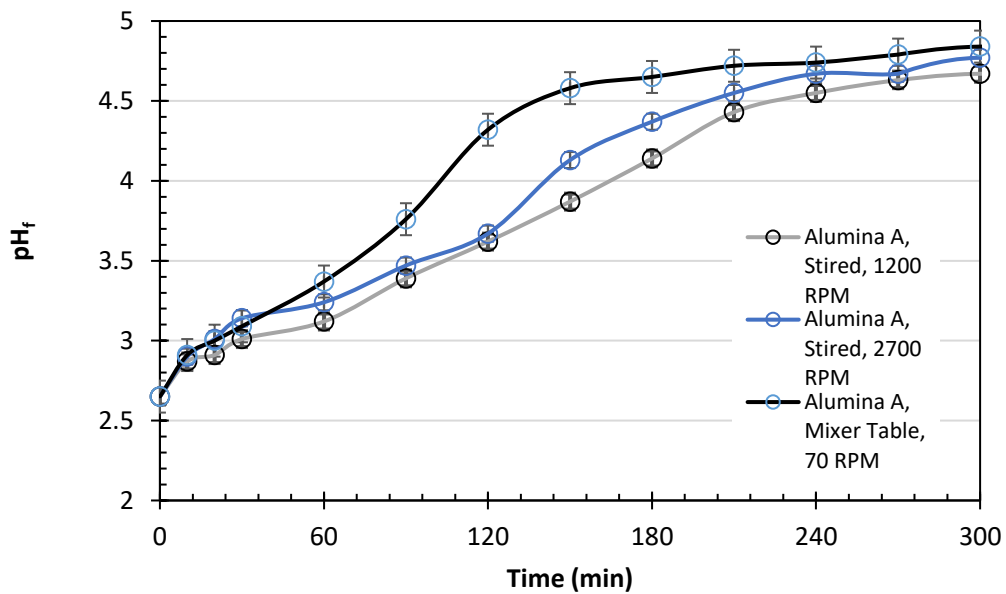


Figure A.5: pH_f kinetics (top) and proton concentration in solution (bottom) for alumina A spheres with a metal free solution at an initial pH of 2.6 as a function of mixing speed.

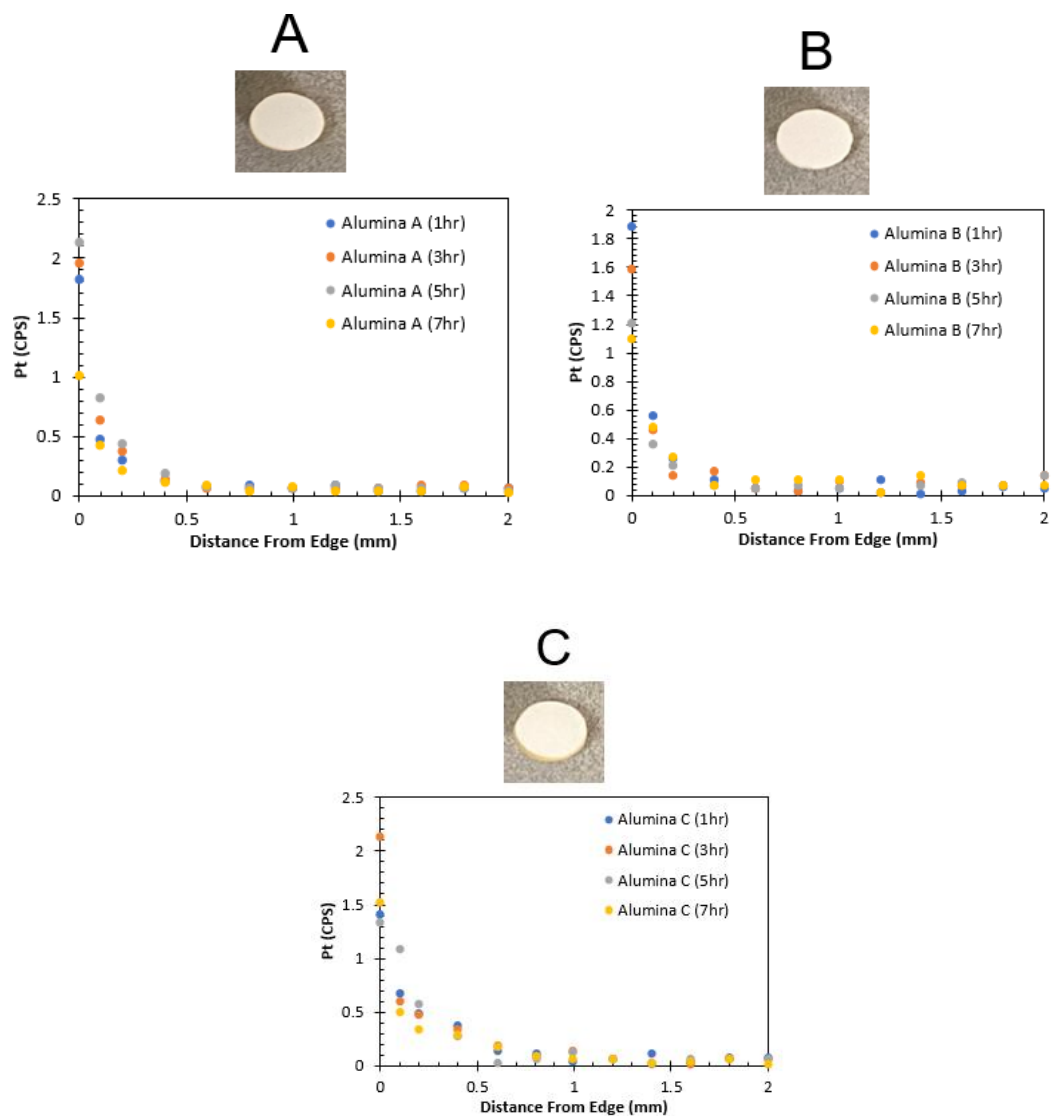


Figure A.6: XRF analysis measuring the counts per second of platinum as a function of distance from the edge of formed support of Alumina A (top), B (middle), and C (bottom) at 200 ppm platinum (CPA).

Appendix B: Norit Carbon

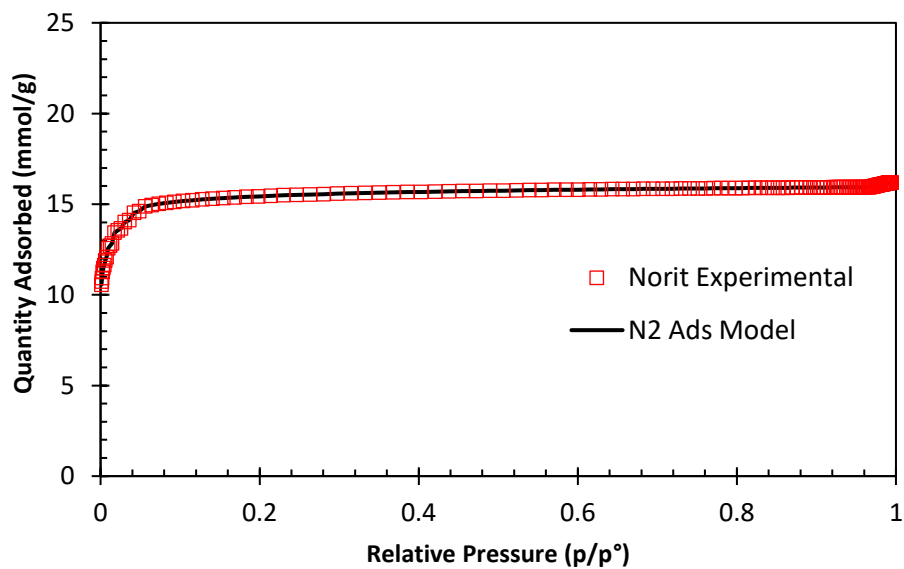


Figure B.1: Experimental adsorption isotherm for Norit carbon compared to a slit geometry N2 adsorption model. The difference between fits suggests good agreement and the absence of mesopores.